INDENTATION CREEP OF ALUMINIUM SILICON CARBIDE (Al-SiC) FOAM

by

TADI PRABHAKAR

DEPARTMENT OF MECHANICAL ENGINEERING

INDIAN INSTITUTE OF TECHNOLOGY, KANPUR

March, 2001

INDENTATION CREEP OF ALUMINIUM SILICON CARBIDE (Al-SiC) FOAM

A Thesis Submitted
in Partial Fulfillment of the Requirements
for the Degree of

MASTER OF TECHNOLOGY

By

TADI PRABHAKAR

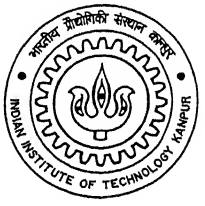

to the

Department of Mechanical Engineering

Indian Institute of Technology Kanpur

March, 2001

CERTIFICATE

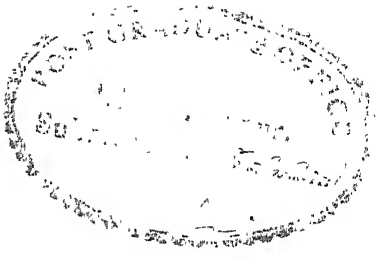

It is certified that the work contained in the thesis entitled **INDENTATION CREEP OF ALUMINIUM SILICON CARBIDE (Al–SiC) FOAM,** by **TADI PRABHAKAR (Roll number: 9910542),** has been carried out under my supervision and that this work has not been submitted elsewhere for a degree.

Om Prakash 5/3/01

Dr. Om Prakash
Assistant Professor
Department of Mechanical Engineering
Indian Institute of Technology
Kanpur-208016.

March 2001.

ACKNOWLEDGEMENT

I wish to express my sincere and heart felt thanks to my thesis supervisor, Dr. Om Prakash whose excellent guidance, affectionate encouragement and inspiration with all-round cooperation have enabled me to bring the work to the present form. The care and freedom showered by him is greatly acknowledged. It is indeed a real pleasure and great privilege to have been associated with him.

I am greatly indebted to all my teachers for their endeavour particularly Dr. Amitabha Mukharjee and Dr. K. Ramesh to make me learn as much as possible. I am thankful to all of my batch mates for providing the right atmosphere to hone my skills.

I would like to thank to all ESA-Lab staff Shri B.D.Pandey, Shri Anurag Goel, Shri Diwakar, Shri Ramsharan Tiwari. I am indebted to Shri B.K Jain, Materials testing lab., ACMS, for his precious and invaluable co-operation during my experimental work.

I wish to express my heartfelt thanks to my friends jayaram, anil, bheema rao, narasimha rao, parthasarathy, jayadeep,saravan,muthu,davel for their endless love, encouragement and endurance which makes my life memorable at I.I.T. Kanpur.

Finally, I am grateful to the Almighty and my parents for what I am today.

-PRABHAKAR

Abstract

This work describes an investigation of the indentation creep relaxation behaviour of Al-SiC foam. This is a novel form of cellular solid based on an aluminium matrix composite with SiC particles. Though some preliminary work has been reported on the mechanical properties of this material both at room temperature and elevated temperature, little is known about its response to contact stresses. Accordingly, this work deals with the high temperature mechanical response of Al-SiC foam under indentation loading.

Creep relaxation tests were conducted by indenting the material to a pre-specified load using a cylindrical punch indenter at various temperatures and the relaxation data obtained. Creep properties of cell wall material were extracted from the relaxation data using a theoretical formulation developed earlier for compression creep relaxation response of metallic foam. The use of this model for indentation creep relaxation has been discussed in relation to low Poisson's ratio and the expected shape of stress field in the material under punch indentation loading. Stress exponent values were obtained in the range 4-13, in close agreement with the properties of the cell wall material. These high values indicate the presence of a threshold stress. The threshold stress appears due to load transfer to the particulates. The activation energy for creep is found to be 40 kJ/mole and indicates significant contribution of surface diffusion.

Contents

List of figures

List of Tables

CHAPTER 1

INTRODUCTION

This work is concerned with the creep-relaxation behaviour of Al-SiC foam under indentation loading. Al-SiC is a new class of cellular solid which incorporates a composite wall construction. In this case, the cell-walls comprise of SiC particles embedded in an Al-Si matrix. The material has a hierarchy of structural features and the overall mechanical response is therefore a complex interplay of processes taking place at various lengths scales. In addition, this material has been developed recently. The low temperature mechanical response of Al-SiC has been studied. However, their behaviour at elevated temperatures, when the cell walls suffer creep deformation, is less well documented.

The following chapters describe the various investigations we have undertaken- the deformation behaviour associated with indentation creep (creep-relaxation) and interpretation of the creep properties of cell wall material from the experimental data. Indentation creep response is relevant for possible applications where this material may be subjected to contact stresses at elevated temperature. The following sections give a brief overview of various topics relevant to this work. These include introduction to cellular solids and metal-matrix-composites, and creep deformation of metal-matrix composites and metallic foam.

1.1 Cellular Solids

1.1.1 Introduction

Cellular solids (or foams) are an important class of engineering materials. They occur in nature (wood, bone shells etc.) and fulfill a variety of functions including high

specific stiffness, high specific strength, transport of fluid (capillary effect through the xylem and phloem in plant tissue), thermal and acoustic insulation, and resistance to catastrophic crack growth (mollusk shells, wood, bone). These attributes are equally desirable in man-made structures/materials. Accordingly, man has made his own cellular solids using a variety of materials including polymers, metals, ceramics and glass. The first cellular solid to be placed on the market was the sponge rubber developed in 1914[1]. Recent development of cost effective processes for the production of metallic foams has increased their potential in a wide range of applications.

A cellular solid is made up of an inter-connected network of solid struts or plates forming the edges and faces of cells. When fraction of voids in a porous body is large, The structure can be described as cellular [2]. Such materials possess low density, are of relatively low-cost and have attractive compressive strength-to-weight ratio. The simplest of the structures are the two-dimensional honey-combs, figure 1.1(a), in which the packing is in a plane area like the hexagonal cells of the bee-hive. In 3-d, the cells are polyhedral, which pack to fill space; such cellular solids are known as foams. Foams may be based on organic, inorganic, or metallic materials; they may be thermoplastic or thermosetting; they may be derived from natural products, or from synthetic products. Foams may be flexible or rigid, e.g. latex foams are flexible whereas urethane foams are rigid. The earliest examples of a large-scale foam-in-place application involving phenolic foam occurred in 1949 when foams were used in aircraft carriers [3]. If the solid of which the form is made is contained in the cell edges only, so that the cells connect through open faces, the foam is said to be open celled, figure 1.1(b). If the faces are solid too, so that each cell is sealed off from its neighbours, it is said to be close-celled, figure 1.1 (c).

The single most important structural feature of a cellular solid is its relative density (ρ^*/ρ_s); that is, the density of cellular material, (ρ^*), divided by that of the solid from which the cell walls are made of, (ρ_s) [4]. The mechanical properties of foams depend strongly on the relative density (figure 1.2). Special ultra–low-density foams have been made with a relative density as low as 0.001. Polymeric foams have relative density typically between 0.05 and 0.2.

1.1.2 Fabrication of Foams

Various techniques are used for foaming different types of solids. Generally, foams are fabricated by dispersing a gas such as air into liquid phase so that a large number of bubbles are formed directly. Some bubbles grow and shrink during the time interval between bubble formation and stabilization. Other bubbles combine to give a small number of large bubbles. Closed-cell foams form if the cell membranes surrounding bubble remain intact. Open cell foams result if some or all membranes rupture. Foams in which a solid or liquid dispersed in a polymer phase can also be manufactured and subsequently removed to get a foam structure. Cellular solids can also be made of bonding together previously expanded spheres or granules. Metallic foams are made by mixing organic beads with metal melt in an inert atmosphere. Glass foams are made by use of blowing agents (often, hydrogen sulphide). Ceramic foams are made by infiltrating polymer foam with a slip (fine slurry of the ceramic in water, or some other fluid); when the aggregate is fired the slip bonds to give an image of the original foam, which burns off. More recently, new forms of foam structures have been developed with highly oriented porosity, figure1.3, [5] as well as those with a composite microstructure [6]. Their properties and potential remains an unexplored area.

1.1.3 Applications of Foams

There are wide ranges of circumstances in which the different properties of foams can be exploited for various engineering applications. The largest is in thermal insulation. This is to exploit the low thermal conductivity of foams. Table 1.1 shows the comparison of thermal conductivity between bulk solids and foams. Closed-cell foams prove to be an excellent material for this. The Second major use lies in cushioning and packaging. This is due to their high energy absorbing characteristics. The possibilities range from automobile bumpers to protective envelopes for air-borne equipments. Open-cell can efficiently be used in acoustics damping. High surface area foams render them as an efficient material for heat exchangers. These foams are extensively used as construction materials in sandwich panels due to exceptional lightweight and high-strength-to-weight

Table 1.1: Comparison of thermal conductivities of foams with bulk solids (Ref. 4).

Material	Thermal Conductivity W/mK
Copper	384
Aluminium	230
Alumina	25.6
Polyurethane foam	0.025
Polystyrene foam	0.04
Cork	0.045

ratio. Foams can also be used in other important engineering applications as porous filters, catalysts in chemical industries and, for high temperature applications (such as ceramic tiles on the outer skin of the space shuttle).

1.1.4 Mechanical behavior of foams

The first comprehensive description of mechanical behaviour of cellular solids is provided in the book by Gibson and Ashby [4]. Overall mechanical response is related to the structure of the cell-wall material as well as the more macroscopic cell-structure. In addition, cellular solids often have a distribution of cell shapes and sizes. Consequently, mechanical characterization must take these factors into account. Most mathematical models generally assume cells of uniform shape and size. Typical compression and tensile stress-strain curves for elastic-plastic and brittle foam are shown in figure 1.4a. In compression all three types of foams show a linear elastic region, followed by a constant plateau stress and finally the region of steeply rising stress. The three regions are associated with different deformation mechanisms. Linear elasticity is due to the cell-wall bending in closed-cell foams and due to the cell face stretching in open-cell foams. Plateau regions is attributed to collapse of cell walls in elastic foams, by formation of plastic hinges in elastic-plastic foam and by brittle crushing in a brittle foam. Due to collapse of cells, many cells come close together, i.e. densification occurs and further deformation compresses the cell-wall material itself. This gives the final, steeply rising

portion of stress strain curve. Tensile deformation for each type (figure 1.4b) of foam is different. For reasons stated above linear elasticity is also observed in tension. In elastic foams, larger strains rotate cell-edges towards the tensile axis, increasing the stiffness of the structure. The cell walls in the plastic foams also rotate towards tensile axis, giving a yield point followed by a rising curve, terminating into fracture. In brittle foams crack nucleate, giving a fast brittle fracture. Fracture occurs by two different mechanisms. Firstly, the cell-walls fracture transversally and crack propagates by breaking walls. Secondly, the crack advances longitudinally in the walls, splitting them into two [7]. In aluminium foams, structural collapse occurs mostly by buckling of cell walls even at low strains [8]. Aluminium foams have almost identical strengths in uniaxial tension and compression [9]. Generally, the deformation concentrates in weak or over-stressed regions and properties to adjacent regions in the form of a deformation band. This type of behavior has been experimentally observed in compression of common cellular materials [10]. This localization of deformation and its propagation in the form of bands also occurs in crystalline compact materials containing impurities that pin dislocations.

The incorporation of second phase in the cell-wall material leads to more complex microstructure and deformation behavior, and is discussed in1.2.3.

1.2 Metal Matrix Composites and Composite Foams

1.2.1 Metal-Matrix-Composites (MMC's)

A composite is a material prepared from two or more different substances that retrain their individual identities and properties. Composites materials generally include constituents that complement each other and are compatible. A structural composite is generally made up of a matrix phase and one or more reinforcement phase(s).

Matrix or base material may be a metal or non-metal, reinforced with agents such as fibers, whiskers and second phase particles. The overall properties depend on the properties of individual phases, their relative amounts, geometrical arrangement and the interaction between the various phases. Metal matrix composites are now a major field of

research as they offer high strength, stiffness and environmental stability of the reinforcing agents. These have evolved over the past 20 years. The primary support for these composites has come from aerospace industry; more recently from automotive, electronic, and leisure (sports goods) industries. At the present time, aluminium, magnesium, nickel based alloys, and ferrous alloys are being used as matrix materials. The aluminium based composites are the only ones that have become widely available and have excellent prospects on account of their low densities, corrosion resistance and availability of information regarding their manufacturability, shaping, service durability etc. various reinforcing materials such as alumina and SiC particulates are being used for these materials.

1.2.2 Al-SiC Foam

Al-SiC foam is based on a metal matrix composite. This material was produced during early researches by bubbling air through molten aluminium (alloy) containing SiC particles [6]. An Al-Si alloy (unspecified composition) was used to make samples for this study. The samples were provided by ALCAN R&D labs (Kingston, Ontario, Canada). The bubbles float to the top surface of the composite to form a closed-cell foam, which is then allowed to solidify. Adjusting the gas flow rate and other process parameters can control cell size of this foam. Figure 1.5 shows samples with different relative densities produced using this technique.

The foam has a closed cell structure. In low density foams, individual cells can feel the presence of neighboring cells during solidification (resulting in thin cell faces) while higher density foams have been found to consist of spherical cavities embedded in alminium matrix. A detailed discussion on the shape of the cells and the effects of SiC particles on the evolution of cell structures is described by Prakash et.al [11]. The cell walls have a complex microstructure (figure 1.6) consisting of voids, cavities, precipitates and micro segregation resulting from dendritic solidification [11]. The SiC particles tend to lie close to the surface of the cell walls (figure1.7). Consequently, the mechanical response of this foam is complex; which is explained in the following section.

1.2.3 Mechanical response of Al-SiC Foam

The mechanical response of Al-SiC foam is related to its cell structure, and also to the microstructure of the material. The introduction of SiC particles leads to changes in elastic properties of cell walls, affecting buckling and collapse loads and alter the behavior of material by introducing new failure mechanisms such as debonding at particle/matrix interface etc. The compression response of bulk Al-SiC foam samples has been studied [11]. The deformation sequence observed was elastic deformation, followed by localised plastic deformation in a few cells .The stress/strain curve (figure 1.8) shows the repeating cycles of yield, collapse and densification of cells. The yield point constitutes particle/matrix debonding and local yield in maximum stressed regions. The stresses are maximum at the mid-section of the longest and thinnest cell edges. The cell membranes do not contribute in bearing of load. However, they do provide stability against buckling of walls. But buckling is not major collapse mode in Al-SiC foam. The collapse of cell walls following localized yielding in a deformation band occurs through membrane tearing and growth of interfacial cracks, resulting in a decrease in stress level. Local densification is then required before deformation may spread to the adjoining cells. Failure thus proceeds with repeating cycles of yield, collapse and densification. Initially successive yield occurs at about the same stress (plateau stress), but with increasing strain there is some amount of densification, which results in increase of stress. The yield stress in plateau region depends on the relative density of foam, with denser foams having a higher yield stress

1.3 Creep

1.3.1 Creep Phenomena

Creep is a continuous deformation with time under an applied load or stress. The strain instead of depending only on the stress depends upon temperature and time also, i.e.

Where, ε is creep strain, σ is applied stress, t is time and T is temperature. This is different from room temperature behavior of most metals and ceramics in which strain is independent of time:

$\varepsilon = f(\sigma)$ (for an elastic-plastic solid)

Usually, creep can occur from 0 °K to melting point (T_m), But, its contribution is significant only at temperatures exceeding 0.4 T_m. Polymers, too, creep even at room temperatures. Most common polymers are not crystalline, and thus have no melting point. For them, the important temperature is the glass transition temperature. Once the temperature exceeds this transition temperature, polymers creep on applying load. Foams made of these materials too, will creep. Even metal-matrix-composites creep and thus the foams based on these are expected to creep as well.

A creep curve plotted as strain vs. time, (for constant applied loads or stress) exhibits three different stages: primary, secondary (or steady state) and tertiary finally leading to fracture (figure 1.9). Metals, polymers and ceramics all show creep curves of this general shape. Primary creep is a transient stage. In secondary stage there is steady increase of strain with time, while tertiary stage has a very high strain rate. Another test, which is characteristic, is the relaxation test. A specimen is loaded rapidly to a fixed strain, and the loads required to maintain that strain is recorded (figure 1.10). It is but natural that there should be a close correspondence between curve and the relaxation curves for any material.

The creep deformation of crystalline materials can take place through various mechanisms such as thermally assisted climb of dislocations (dislocation creep), or through stress-directed diffusion mass transfer (diffusion creep). A phenomenological description of creep is given by a creep-law:

$$\dot{\varepsilon} = A\sigma^n \exp(-Q/RT) \qquad 11$$

Where, $\dot{\varepsilon}$ is the steady state strain-rate, A is a constant, σ is the applied stress, n is the stress exponent, Q is the activation energy for creep, R is the universal gas constant, and T is the temperature at which the creep test has been conducted. The properties of a material are often described in terms of the values of n and Q. The stress exponent lie between 3–6 for dislocation creep for most metals. Under conditions of stress and temperature where diffusion creep dominates, the stress exponent has a value equal to 1. Figure 1.11 shows the ranges of applied stress and temperature over which different mechanisms dominate in aluminium. The dependence of the creep rate on temperature is Arrhenius in nature. The activation energy for creep is similar to that for self-diffusion since dislocation creep as well as diffusion creep is made possible through (lattice) diffusion of atoms. Under certain conditions, creep may be controlled by diffusion of atoms, along dislocations through core or grain-boundaries, and the appropriate values of activation energy for creep then correspond to dislocation–core or grain boundary diffusion. The former yields $Q_{\perp} \cong (1/2)\ Q_{sd}$ and the latter $Q_{sd} \cong (1/3)\ Q_{gb}$, where $Q_{\perp}$ is activation energy for diffusion through dislocation core, Q_{gb} is the self-diffusion activation energy for grain-boundary diffusion.

Interpretation of creep behavior of metallic alloys in terms of the power-law creep equation often yield very high values of stress-exponent (in the range of 8–25) and activation energies about 3–5 times Q_{sd}. This is rationalized in terms of a threshold stress in the material, which must be overcome in order that creep deformation may take place. The threshold stress can be identified with long-range internal stress field set-up due to the interaction of dislocations with grain boundaries (dislocation pile ups) or the evolution of dislocation substructures or the Orowan-type strengthening due to pinning of dislocations at particles/precipitates etc. Various models have been proposed to account for the resulting increase in the values of the power-law stress exponent [12–17]. A feature, common to all these models is that the creep is driven by an effective stress, which equals the applied stress minus the threshold stress. Applying this correction to the creep data usually yields n values equal to that of the unalloyed/unreinforced matrix and Q values close to that of self-diffusion.

Table 1.2: Comparison of threshold stress for different composites.

Composite	T (K)	Threshold Stress (Mpa)
Al-Mg-10 Vol% SiC_p (Ref.27)	573	35.4
	623	34.2
6061 Al-17.4 Vol% SiC_w (Ref.18)	505	70.2
	561	49.2
6061 Al-26.5 Vol% SiC_p (Ref. 18)	561	24.2
6061 Al-15 Vol% SiC_w (Ref.18)	573	47.6

1.3.2 Creep Response of MMC's

Creep of composite materials strongly depends on the temperature and applied stress. It has been observed that stress exponent of the steady state creep of 6061 Al-SiC_w composite is approximately 20.5 and it remains essentially constant within the range of test temperatures [18]. Activation energy for this composite has been found to be approximately 390 KJ/mole; nearly three times as high as the activation energy for self-diffusion of aluminium which is 142 KJ/mole [19]. Such high values of stress exponent and activation energy are also observed for other systems such as sintered aluminium powder containing fine alumina particles [20].

The origin of the threshold stress for pure Al-SiC_p composites has been discussed in terms of various possible mechanisms, such as dislocation-particle interaction, internal stress associated with sub-grains, and load transfer to the stiffer reinforcement phase [21]. Load transfer to the SiC particulates has been suggested as an origin of threshold stress in pure Al-SiC_p composite. It is noteworthy that the threshold stress is considered to be constant at any given temperature and not a function of applied stress. Due to their larger length and higher load-bearing capacity of SiC whiskers, the threshold stress for SiC-whisker reinforced composites is expected to be higher [Table 1.2]. An important parameter for load transfer is the nature of interface between the matrix and the

reinforcements. The nature of the interface usually depends on the compatibility of the reinforcement with matrix and also on the processing of the composite. Thus, applied-stress-independent load-transfer model suggested for pure Al-SiC_p composite [21] should also include the nature of interface to accurately predict the threshold stress for creep in composites.

1.3.3. Creep Response of Metallic Foams

The problem of creep behaviour of cellular solids has been discussed in [1], but for the relatively simple case of uniform cell shape and size, in a 2D honeycomb structure. The creep relaxation behaviour of composite foam (Al-SiC) has been described in [30], considering distribution in cell size and the non-uniform structure. Khare et. al. [30] developed a model for the creep relaxation behaviour in terms of the geometrical structure and creep properties of cell-wall material. They carried out a set of experiments on compression creep relaxation of Al-SiC foam to assess the validity of the model. Good agreement was obtained between theory and experiments. The theoretical framework developed has been summarised in Appendix A and B.

The stress exponent for the cell material is given by [30] by

$$\frac{1}{P^{n-1}} - \frac{1}{P_0^{n-1}} = kt \qquad 1.2$$

where P_o is the initial load, P is load at time t, n is the stress exponent of the cell wall material and k is a constant which takes into account the geometrical details and the statistics of the cell wall distribution..

The expression for activation energy for creep is

$$\ln(k^{**}) = \ln(JE) - \left(\frac{Q}{RT}\right) \qquad 1.3$$

The activation energy, considering temperature dependence of young's modulus is

$$\ln(k^*) = \ln(J) - \left(\frac{Q}{RT}\right) \qquad 1.4$$

The activation energy can be obtained from a plot of ln (k**) or ln (k^*) against 1/T. The various notations are as defined in Appendix B.

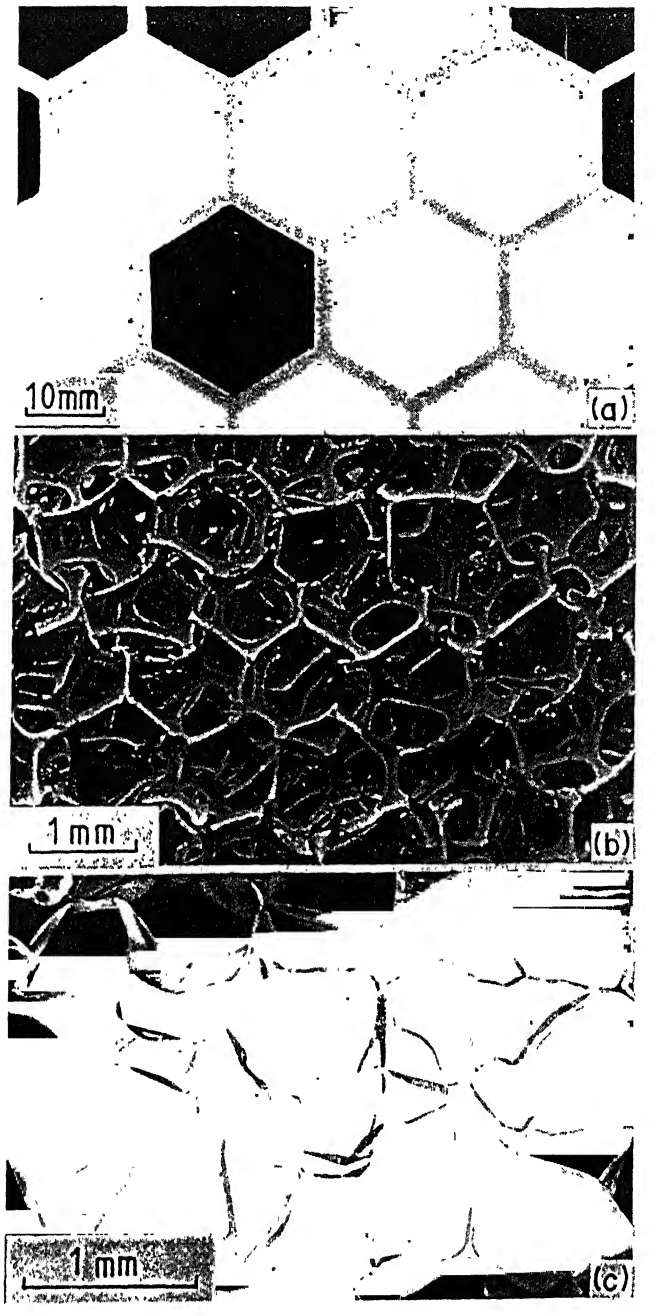

Figure 1.1. The structure of dofferent types of cellular solids: (a) 2-d Honey comb (b) 3-d open celled foam and (c) 3-d Closed-cell foam (ref.4).

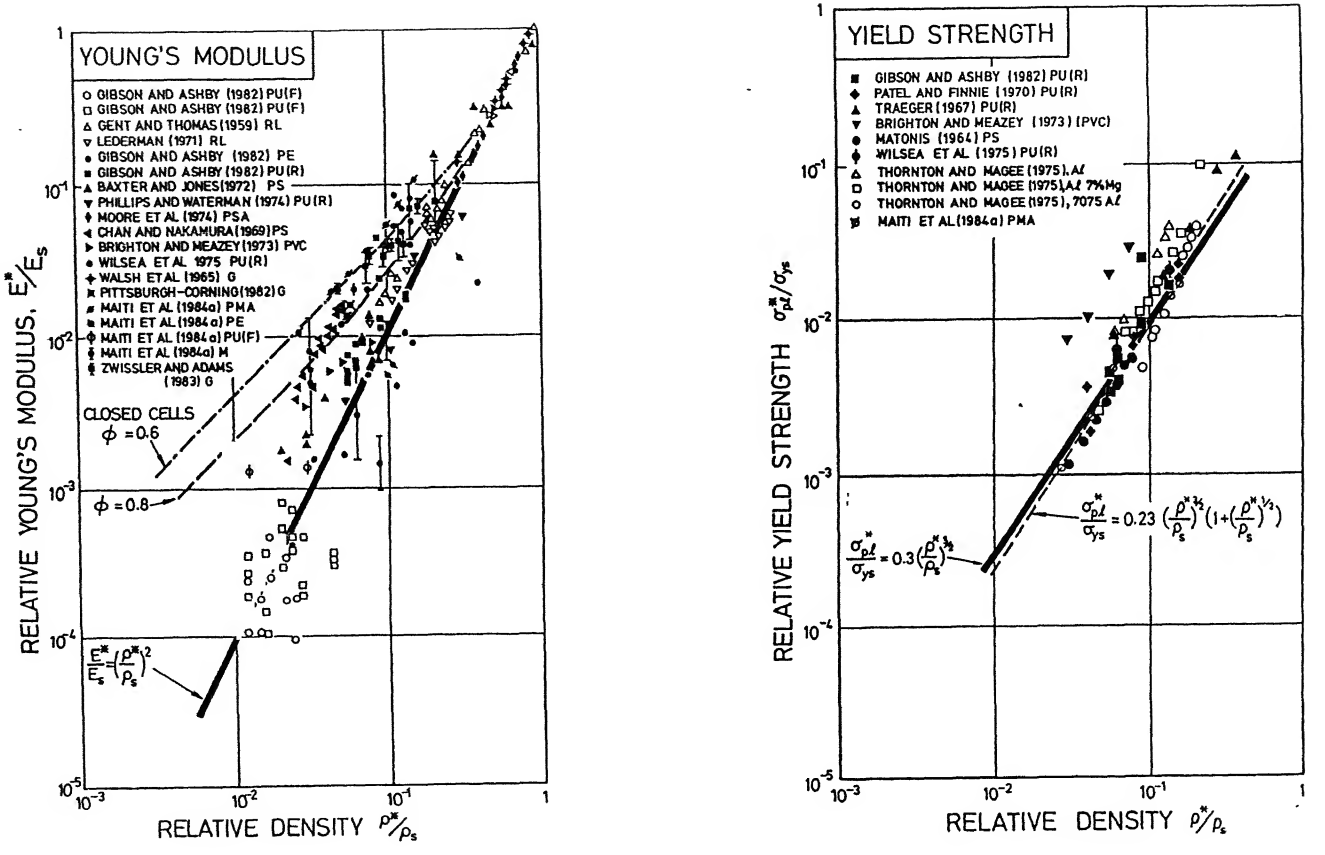

Figure 1.2 Data of foams for (a) Young's modulus and (b) Yield strength, plotted against relative density, ρ^*/ρ_s. Solid line represents open-cell foams: Dashed line represents closed-cell foams (ref.4)

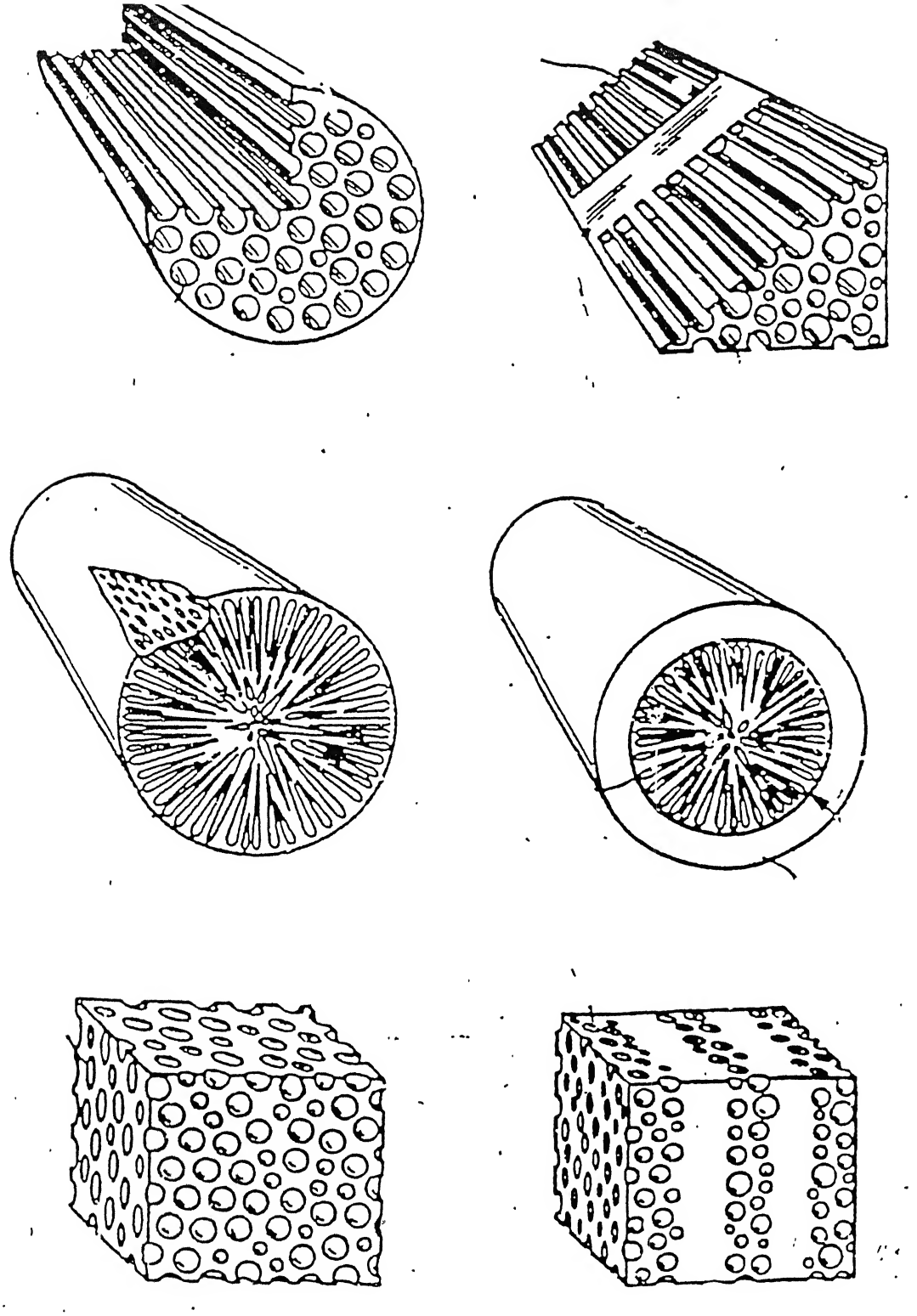

Figure 1.3. Schematic diagram showing cellular solids with highly oriented porosity produced using gas-eutectic reaction (ref.5).

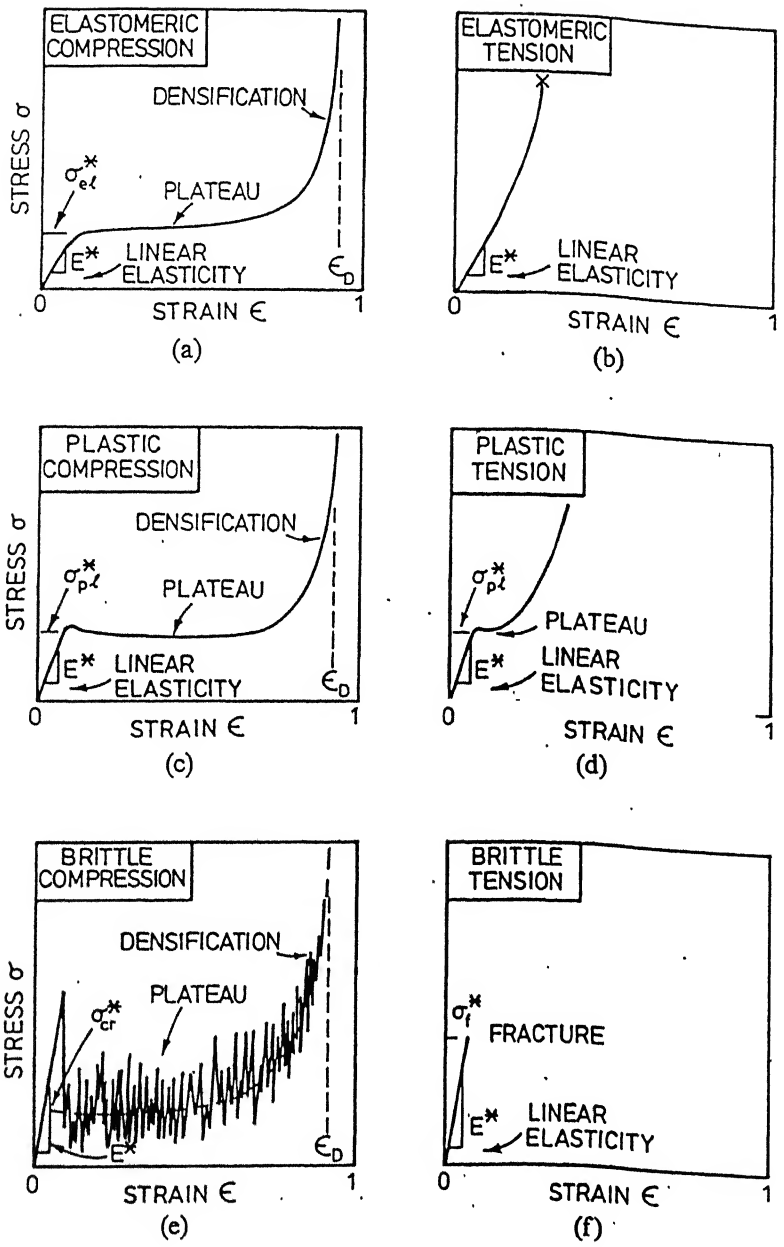

Figure 1.4. Schematic stress-strain curves for elastomeric, elastic-plastic and elastic-brittle foams under (a) Compression and (b) Tension (ref.4)

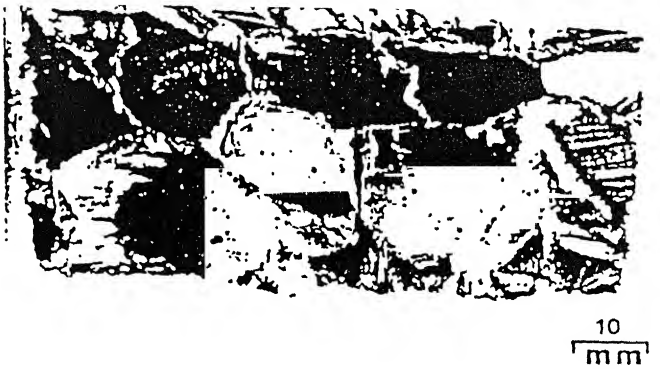

(a)

(b)

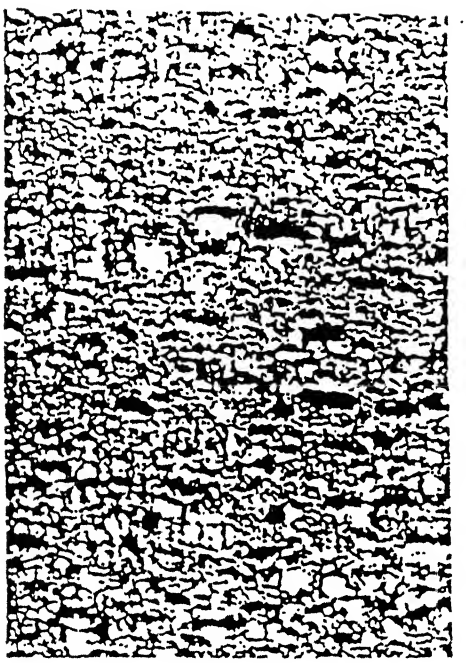

(c)

Figure 1.5: Macrostructures of Al-SiC foams with relative densities (a) 0.04 (b) 0.1 and (c) 0.2 (ref.11)

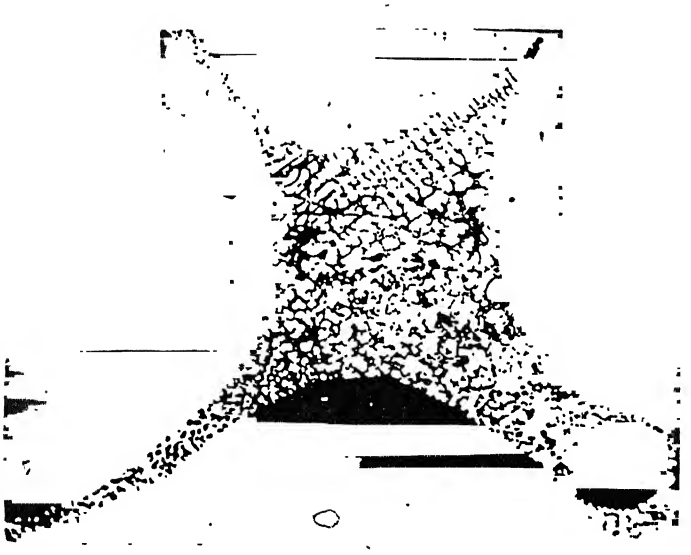

Figure 1.6. Optical micrograph of cell edges in Al-SiC foam showing distribution of SiC particles (ref. 11).

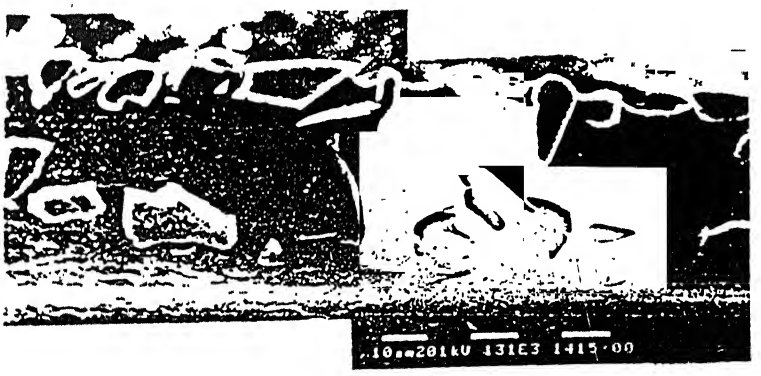

Figure 1.7. SEM micrograph showing distrbution of SiC particles close to surface of a cell wall in Al-SiC foam (Ref.11).

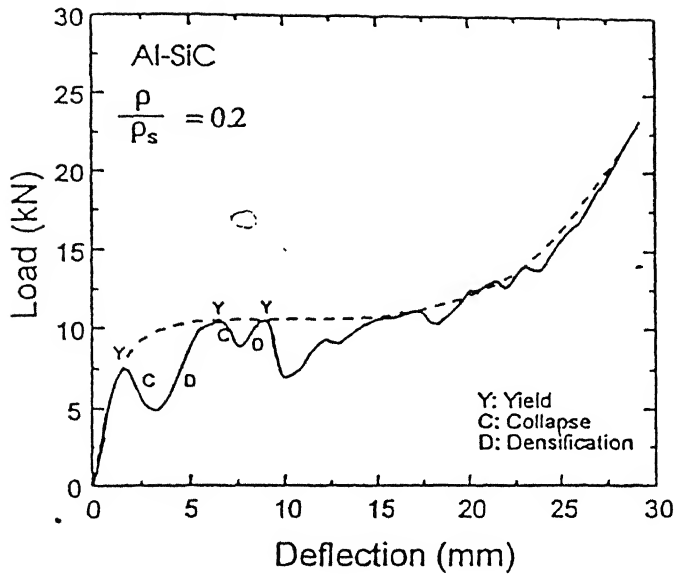

Figure 1.8. Load/deflection curve of Al-SiC foam. The dashed curve represents the locus of yield points (ref.11).

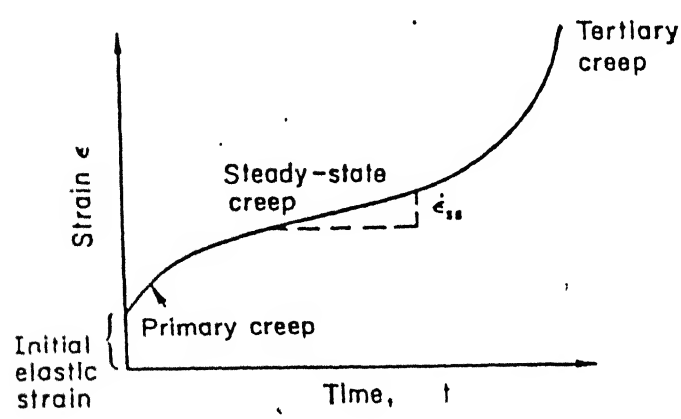

Figure 1.9. Schematic diagram of uniaxial cree-curve for crystalline materials. Stage I, II, and III denote primary, secondary and tertiary creep.

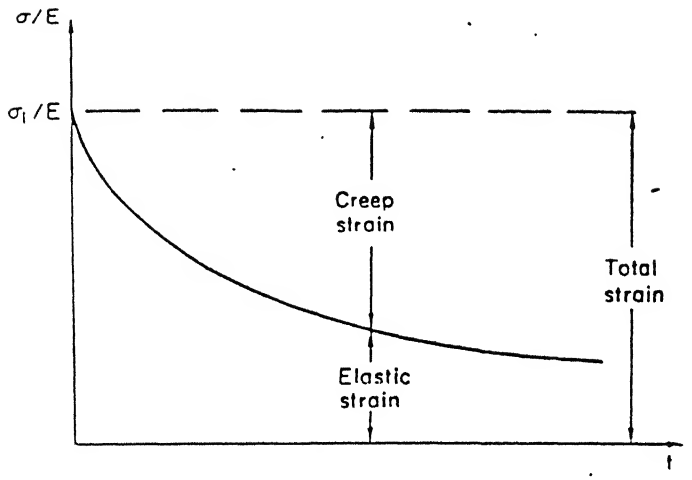

Figure 1.10. Schematic creep relaxation cureve

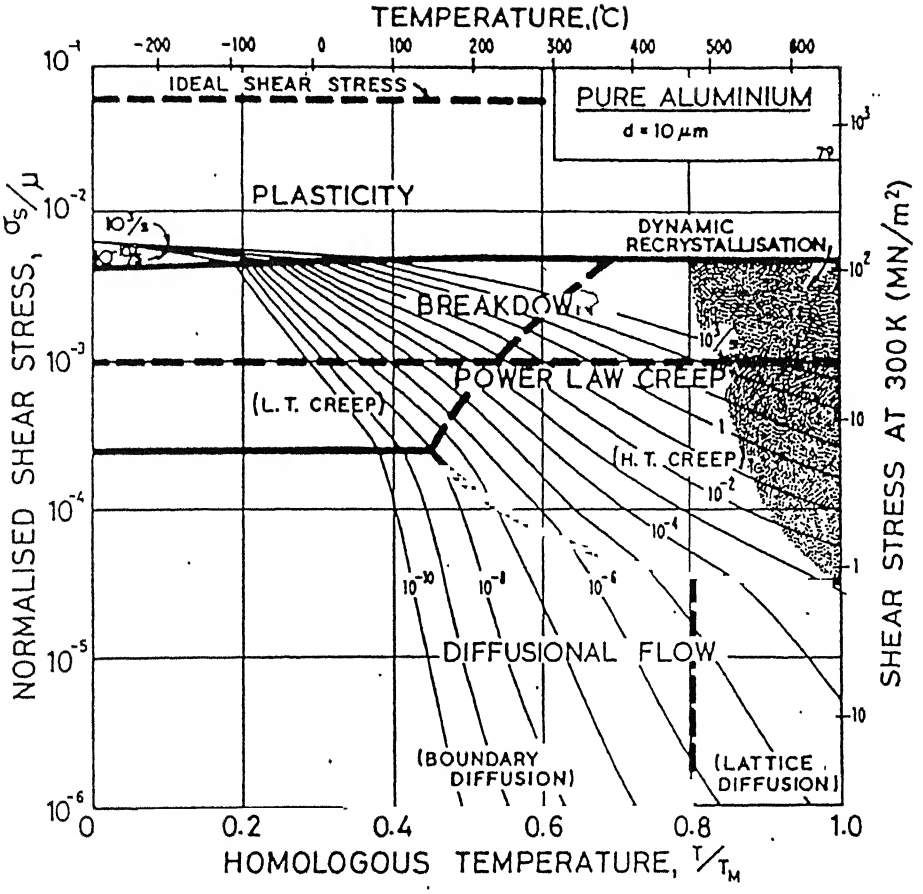

Figure 1.11. A deformation Mechanism map of pure aluminium of grain size 10 μm showing the deformation mechanism s dominate in various ranges of a applied and temperatures (ref.19).

CHAPTER 2

EXPERIMENTAL DETAILS

The relaxation behaviour of Al-SiC foam under compression had earlier been described by Khare [29]. The present work is concerned with the creep response of this material under indentation loading. A cylindrical punch indenter has been used for this purpose. The indentation tests may be performed in the following different ways:

- Type I test: The depth of indentation may be recorded as a function of time for given value of load and temperature.
- Type II test: The variation of stress (or load) with time be recorded for an imposed indentation velocity.
- Type III test: The relaxation of stress (or load) may be recorded as a function of time for a given temperature and imposed initial strain (depth of indentation).

Type I tests cannot be performed because of non-availability of depth sensing indentation machines. Type II tests are feasible in general, but are not well suited for foam materials because, under imposed strain-rates, it may be difficult to limit maximum stress to safe levels in terms of formation and propagation of microcracks in the cell walls. The latter would interfere with the overall deformation making it difficult to delineate the creep properties from the observed response. Type III tests enable us to record load relaxation subsequent to any imposed initial load; the latter may be chosen so that the initial strain is within elastic limits, precluding the possibility of fracture processes interfering with the creep response. Accordingly, creep relaxation tests were perfumed in the present study.

In the following sections, we give details about specimen preparation and the creep relaxation test.

2.1 Sample preparation

To ensure that the observed mechanical response is representative of the bulk material, the sample should consist of a large number of cells and the indenter diameter should be large. On the other hand, there are restrictions on the sample size imposed by the furnace size and the testing machine. A sample size (cylindrical samples) of length, l = 36 mm and diameter, ϕ = 34 mm (figure 2.1) was therefore chosen to satisfy both these requirements. The samples contained on average about 500 cells (about 70 cells in any cross-section plane) as shown below:

$$No.\ of\ cells = \frac{Total\ Volume}{Volume\ of\ one\ cell}$$

Thus, with an average cell diameter (2r) of 5 mm,

$$No.\ of\ cells = \frac{\pi \frac{\phi^2}{4} l}{\frac{4}{3} r^3 \pi} \sim 500$$

The foam samples initially available for this work were of cylindrical shape, having length, l = 120 mm and ϕ = 44 mm. These samples were machined to the required size on a center lathe machine at a speed of about 15 mpm. with a H.S.S. tool. It was observed that low machining speeds resulted in poor finish and high machining speeds resulted in rapid wear of the cutting tool edge. The later is presumably due to the presence of SiC particles in this material. A collet of mild steel (M.S) having a taper of 1 in 40 was fabricated for holding the material on lathe. This was done to prevent any damage to the

material through the indentation marks of the chuck. Care was taken that the ends of the machined edges were parallel and square.

2.2 Indentation Creep Relaxation Test

The punch indenter was a cylindrical piece of alumina, 1cm long and 1cm in diameter. The large diameter of the indenter leads to relatively large contact area and many cells contributing the creep response of the foam material.

These tests were performed on an MTS 810.12 materials testing machine. An electrical furnace (temperature range 20–1000 °C) was installed on the machine and the sample was loaded on it by moving the cross-head (figure 2.2). The indenter was placed between the sample and the top platen of the machine. Care was taken to prevent any non-axiality of loading. The temperature level in the middle zone of the furnace was monitored using three chromel-alumel thermocouples. The heating rate was controlled by adjusting the current flow through the heating coils and the temperature was allowed to stabilize (± 2 °C) before the experiment was started. The response of the furnace in terms of thermal stability was evaluated prior to the series of experiments on creep. It was found that the furnace gave stable thermal response after about 45 minutes of heating. A couple of asbestos plates were placed over the furnace (around the cross head) to minimize radiation heating of the surrounding structures. As this material was expected to bear an elastic load of about 50 kg. [11], a load cell with 100 kg. capacity was used for the experiment.

These creep relaxation tests were carried out at various temperatures in the range of 300 °C–500 °C. The upper limit was based on the consideration of melting point of aluminium, which is 660 °C and the phase diagram for Al-Si alloy, which shows a eutectic temperature at about 570 °C (figure 2.3). Some scatter in creep data was observed during experiments due to thermal drift in the load cell. This was noticed by monitoring the temperature of the rod connecting the top platen to the load cell. So

Table 2.1: Control parameters during creep test

Temperature	300°K
Load 10% (10V = 10 kg)	46 kg
Chart Speed	0.5 cm/min
Full Scale Deflction (FSD)	1 mm
Stroke control, R	$6*10^3$ sec

Table 2.2: Control parameters during relaxation tests.

Chart Speed	1 cm/min
Full Scale Load (FSD)	50kgs
load (10 v = 50 kgs)	10%
Chart Speed	0.5 cm/min.
Stroke (10 V = 10 mm)	10%
Stroke Control, R	6×10^3 sec

cooling water is circulated through the cross-head. Different samples were initially loaded to a predetermined level of load (which was less than the yield strength at the corresponding temperature, as shown in fig 2.4) and the cross-head was stopped (to maintain a constant strain throughout the experiment). Following this, load-relaxation with time was recorded. The parameters controlled during these experiments are tabulated in Table 2.1 and Table 2.2.

2.3 Microstructural Characterization

Initially, one cell wall segment was separated out from the sample and observed under SEM to characterize its microstructure. Similarly, samples, which had undergone creep deformation, were also characterized. Small segments which had broken off from the bulk samples during the creep test were cleaned in an ultrasonic cleaner using acetone media for about 10 minutes to remove dirt/dust particles, oily layer etc. The cleaned samples were mounted on brass by applying silver paint. The samples were then sputtered with gold in the sputtering unit. Sputtering was necessary otherwise excessive charging of the SiC particles would take place in the SEM. Sputtering was carried out after a vacuum of about 0.1 Torr. was attained in the sputtering unit. Total sputtering time was about 40 minutes. The sputtered samples were then observed in the JEOL [JSM-840A, JAPAN] scanning electron .

Figure 2.1. Photograph of Al-SiC foam samples used for creep tests.

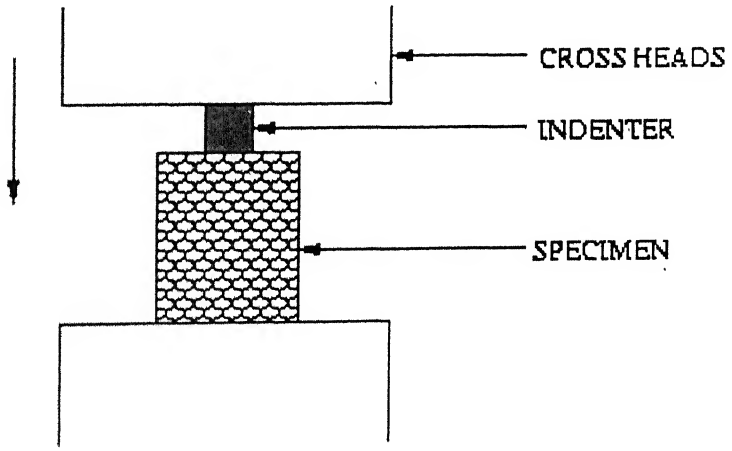

Figure 2.2. Sample loaded between cross-heads on MTS.

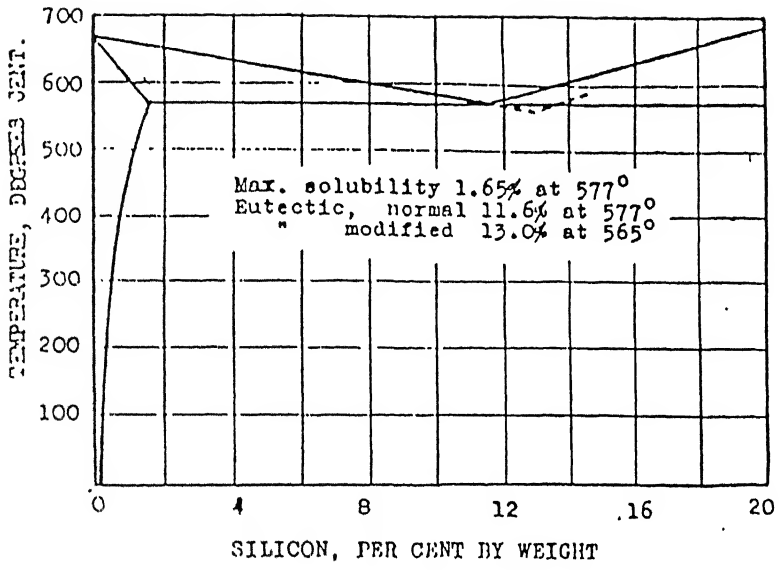

Figure 2.3. Phase diagram of an Al-Si system

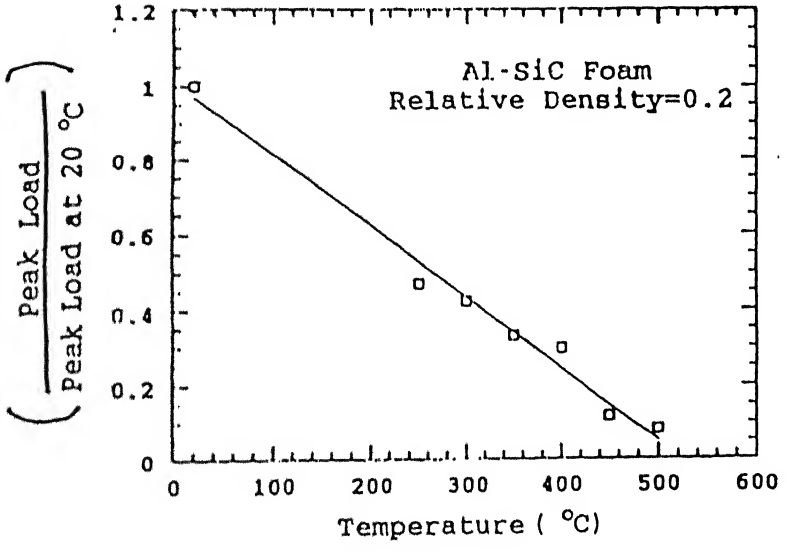

Figure 2.4. Temperature dependence of strength in Al-SiC foam (ref. 22).

CHAPTER 3

RESULTS AND DISCUSSION

3.1 Structure of Al-SiC Foam

As noted in section 1.2.2 a hierarchy of structures exists in Al-SiC foam. These can be grouped into two categories: cell structure (geometrical) and microstructure. The geometrical features include cell shape and size, distribution of cell size, and, defects and flaws in the cell structure. The microstructural features include the size and distribution of SiC particles, grain size etc. The overall mechanical response of such solids is determined by the interaction between these factors for a given loading geometry. At macroscopic scale, Al-SiC foam has a closed structure, the shape of the cell is found to be closely related to the relative density of the foam (see figure 1.5). In general, the cells are made of cell edges (struts) and cell walls (thin membranes) providing a closed cell structure. The cells are polyhedral in shape. The shape of the majority of the cells can be described as an irregular dodecahedron, consisting of 12 pentagonal faces, 30 triangular prismatic rods (edges) and 20 vertices [11]. At cell edges, where cell walls meet, surface tension forces cause the liquid-gas interface to be curved in an arc called plateau border. The edges have a continuously decreasing cross-sectional area from the nodal points (where they meet the other edges) towards their mid span.

Figure 3.1a shows that the walls are often wrinkled, indicating that surface tension forces have-not played much role in shaping the cells. Some particles can also be seen lying close to the surface (figure 3.1b). Dodecahedrons are not space filling structures and, accordingly, tetrahedral cells are present in positions where four adjacent cells meet. Two adjoining cells share a wall and three adjoining cells share a prismatic rod. The edges are slightly thicker than the cell walls. The fractured edge of the sample used for

microscopy showed (figure 3.1 b, c), ductile tearing of aluminium matrix. At a macroscopic scale, the material has a structure as described in section 1.2.2.

A sample was exposed to high temperature of 200°C for about one hour, cooled down, and its microstructure studied (see figure 3.2). The cell wall surface shows the formation and growth of cracks at the interface (debonding) (figure 3.2a). This demonstrates that the interface is weak. The fractured edge (figure 3.2b) of the sample shows ductile failure in aluminium matrix.

3.2 Creep Relaxation Response

The indentation creep relaxation response of Al-SiC foam was obtained at various temperatures and is shown in figures 3.3-3.6. The data was then analysed to determine stress exponent and activation energy for creep using the model described in Appendix A and B. It is assumed here that the compression creep relaxation model is applicable to indentation as well. The justification for this assertion is discussed in section 3.2.4.

3.2.1 The Stress Exponent

The stress exponent for creep at various temperatures is calculated using equation A.17. It ranges between 4–13 as shown in table 3.1, which agrees closely with the data for solid Al-SiC composites [18]. These values are much higher than stress exponent for aluminium (n=4) indicating that incorporation of SiC particles lead to improvement in creep properties. It also suggests the presence of threshold behaviour, and is discussed in section 3.2.2. The effect of temperature on the stress exponent is shown in figure 3.7. This is also consistent with the presence of threshold behaviour.

Table 3.1: Stress exponents Derived from relaxation creep of Al-SiC foam

Temperature (^{0}C)	Initial load P_o (KN)	Stress exponent (n)
300	0.367	12.9
400	0.22	7.2
450	0.1	6.5
500	0.1	4.5

3.2.2 The Threshold Stress

In regard to the origin of threshold type behavior in creep response of these materials, various mechanisms based on the interaction of dislocations with particles (such as Orowan looping, local climb, and general climb) are ruled out on account of the large size of the particles and large inter-particle spacing. It has been proposed [21] that load transfer to particulates can be one of the possible reasons for the threshold behavior in creep of Al-SiC discontinuous composites. If the externally applied load is shared between the matrix and the particulates, the creep deformation of the matrix phase will be driven by an effective stress equal to the applied stress minus the stress transfer to the particles. An important condition for efficient load transfer is the nature of the particle/matrix interface. The behavior of interface is based on the processing of composite. In the absence of any theoretical framework, it is impossible to make any quantitative estimate, but a few general comments about the role of the interface are in order. If the particle/matrix interface is strong, load transfer from matrix to the particles will leads to lower effective stresses under which creep deformation can take place. This leads to very high apparent stress exponents for creep [28]. Also, the threshold stress will be proportional to the applied stress at any instant, since the portion of load transferred is a function of the geometry and the relative elastic properties of the two phases (a result similar to that obtained using shear-lag analysis commonly employed in fiber reinforced composite [25]). With increasing temperature as the interface weakens, the load is transferred less efficiently. Accordingly, one expects lower values of the stress exponent

for creep. The actual variation of the stress exponent for creep with temperature of Al-SiC foam is plotted in figure 3.7 and is found consistent with this view.

3.2.3 Activation Energy for Indentation Creep

The activation energy for indentation creep was determined using the following equations, as described in Appendix B.

$$k^* = \frac{k}{f(n)E} = J\exp\left(\frac{-Q}{RT}\right) \qquad 3.1$$

$$\ln(k^*) = \ln(J) - \left(\frac{Q}{RT}\right) \qquad 3.2$$

If the temperature dependence of E is taken to be negligibly small,

$$k^{**} = \frac{k}{f(n)} = JE\exp\left(\frac{-Q}{RT}\right) \qquad 3.3$$

$$\ln(k^{**}) = \ln(JE) - \frac{Q}{RT} \qquad 3.4$$

The details of the above models are given in Appendix A and B. Values of E, k, k*, k** were determined and given in tables 3.2 and 3.3 for Al-SiC foam.

Table 3.2. Values of various parameters used for calculation of activation energy.

T °C	T/Tm	E×10^{11} (N/m2)	n	k	1/T (1/K)×10^3	k*
300	0.61	0.573	12.9	60580.67	1.745	10.59
400	0.72	0.541	7.20	5834.769	1.486	66.71
450	0.523	0.523	6.50	6702.32	1.383	13514
500	0.597	0.510	4.52	814.7059	1.294	82.2

Table 3.3. Values of various parameters at different temperatures used for calculation of activation energy.

T °C	T/T_m	n	k	1/T $(1/K)\times10^3$	k^{**}
300	0.61	12.9	60580.67	1.745	6.06
400	0.72	7.20	5834.769	1.486	36.09
450	0.523	6.50	6702.32	1.383	70.68
500	0.597	4.52	814.7059	1.294	40.87

The temperature dependence of elastic modulus (E) is small and is not likely to effect the results much, as shown below:

The temperature dependence of shear modulus is given by the following equation [19]:

$$\mu=\mu_0\left(1+\frac{T-300}{T_m}.\frac{T_m}{\mu_o}\frac{d\mu}{dT}\right) \qquad 3.7$$

Where,

μ_0 = shear modulus at 300K

$= 2.54 \times 10^4$ Mpa (for aluminium)

T_m = melting point

= 933 K (for aluminium)

At two different test temperatures, say $T_1 = 573$ K and $T_2 = 723$ K, we get the ratios as:

$$\frac{\mu_{573}}{\mu_{753}}=1.127 \qquad 3.8$$

We know that: $E = 2\mu(1+\nu)$, where ν is the Poisson's ratio. If ν is assumed to be constant with temperature, so $E \alpha \mu$. Thus,

$$\frac{E_{573}}{E_{723}}=1.127 \qquad 3.9$$

i.e. a variation of 12 % is recorded in the value of elastic modulus when the temperature changes in the specified range. Also, from the results obtained, we can see for the same temperature range as specified above, that the variation in f(n) is about 6000%.

$$\frac{f(n)_{573}}{f(n)_{723}}\sim 6000 \qquad 3.10$$

Figure 3.8 shows the Arrhenius plot when temperature dependence of E is considered to be negligibly small and figure 3.9 shows the Aarrhenius plot when temperature dependence of E is also taken into account. The activation energy for creep, Q, is found from a plot of $\ln(k^{**})$ or $\ln(k^{*})$ against 1/T; The measured activation energies are 41 KJ/mol and 43 KJ/mol respectively. The difference between the two values is only about 4%.

As compared to the activation energy for lattice diffusion of Al (Q_v = 145 KJ/mol) the activation energy for indentation creep of Al-SiC foam is $Q_c = 0.3\ Q_v$. Such low value of Q_c is expected and can be explained on the basis of the role of surface diffusion. Since indentation creep involves localised deformation, surface diffusion along the interface between the indenter and the material will contribute to the overall deformation. The activation energy for surface diffusion (Q_s) is typically about 5-20% of Q_v [30], giving Qs = 7-29 KJ/mol. The experimental value of Q_c is a net effect of Q_v and Q_s and is therefore expected to lie between Q_s and Q_v.

3.2.4. Stress Field beneath the Indenter

In section 3.2.1 it was asserted that the theoretical model developed for compression creep relaxation is applicable to indentation creep relaxation as well. This may be explained in terms of the low poisson's ratio of cellular solids and the expected shape of the plastic zone in the material beneath the indenter. Cellular solids exhibit very low value of Poissons ratio, often close to zero [4]. The presence of open spaces allow deformation of material without associated transverse deformation i.e. there is no constraint to transverse deformation offered by the surrounding material . So, effectively, the material under the indenter is subjected to compression loading.

Further insight is offered on the basis of stress field in indentation loading. The shape of the plastic zone under indentation loading of elastic-plastic half-space was described by Bhattacharya and Nix [31]. Based on FEM simulations, they showed that the shape of the plastic zone depends on the ratio E/σ_y value. If this value is high (for example E/σ_y = 157 for aluminium), the deformation mode is radial compression, whereas for

materials with low values of E/σ_y, deformation occurs by cylindrical compression (for example $E/\sigma_y = 21$ for silicon), see figure 3.10. For intermediate values, a combination of cylindrical and radial compression is found to take place. The shape of the plastic zone is found not to change with depth of indentation. The following paragraph shows an estimate of the ratio E/σ_y for Al-SiC foam.

As a first estimate, if we use E and σ_y values of bulk Al-SiC foam, we obtain $E/\sigma_y = 178$. Indicating that deformation in Al-SiC foam should take place in radial compression mode. However, since we are considering indentation deformation and not bulk deformation, we must use a modified estimate of σ_y. Since indentation hardness is generally 3 times the uniaxial strength, we obtain $\frac{E}{(\sigma_y)_{ind}} = 59$. However the relation $(\sigma_y)_{ind} = 3\ \sigma_y$ may not be applicable to cellular solids.

A more reliable estimate may be based on scaling laws of mechanical properties for cellular solids. As shown by Gibson and Ashby [4],

$$\sigma_y^* = \left(\frac{\rho^*}{\rho_s}\right)^{\frac{3}{2}} .\sigma_s \qquad 3.11$$

where σ_y is the yield stress, ρ^* is the density of cellular solid, ρ_s is the density of the cell wall material and σ_s is the strength of the cell wall material. Similarly,

$$E^* = \left(\frac{\rho^*}{\rho_s}\right)^2 .E_s \qquad 3.12$$

where, E^* is the elastic modulus of foam material and E_s is the elastic modulus of cell wall material.

Since indentation hardness is a measure of the surface response of the Al-SiC foam, appropriate value of $\left(\frac{\rho^*}{\rho_s}\right)_s$ in equation 3.11 should be the surface relative density. Surface density is related to volume density through the expression (see Appendix C)

$$\left(\frac{\rho^*}{\rho_s}\right)_{surface} = \left(\frac{\rho^*}{\rho_s}\right)^{\frac{2}{3}}_{volume} \qquad 3.13$$

The elastic modulus should depend on the volume density since E is a measure of resistance to deformation by the entire sample. Therefore, we obtain from equations 3.11, 3.12, and 3.13,

$$\frac{E^*}{\sigma^*} = \frac{1}{0.3} \cdot \frac{\left(\rho^*/\rho_s\right)^2_{vol}}{\left(\rho^*/\rho_s\right)^{3/2}_{surface}} \left(\frac{E_s}{\sigma_s}\right) \qquad 3.14$$

In the present study relative density of the Al-SiC specimen $\left(\frac{\rho^*}{\rho_s}\right)_{vol}$ is 0.1 and the ratio E/σ_y for aluminium is 157. Therefore, $\left(\frac{\rho^*}{\rho_s}\right)_{surface} \cong 0.2$ and $\frac{E^*}{\sigma^*} \cong 45$

The relatively low value of this ratio indicates that indentation deformation in Al-SiC foam would be one of cylindrical compression and not radial compression.

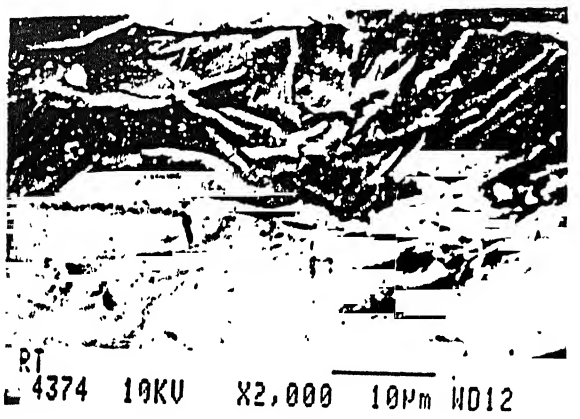

(a)

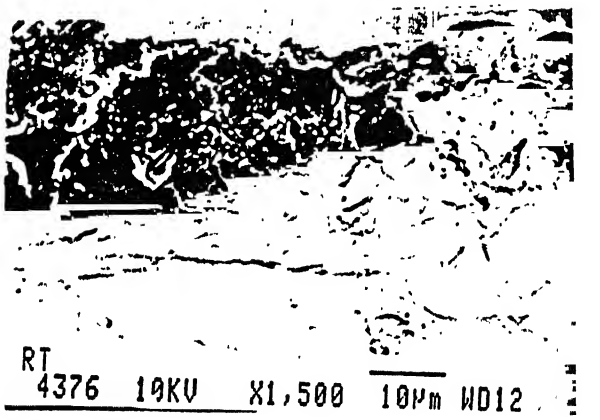

(b)

(c)

Figure 3.1. Micrographs of Al-SiC foam at room temperature showing (a) surface characteristics (b) fractured edge (c) enlarged view of a section of fractured edge in(b)1500X.

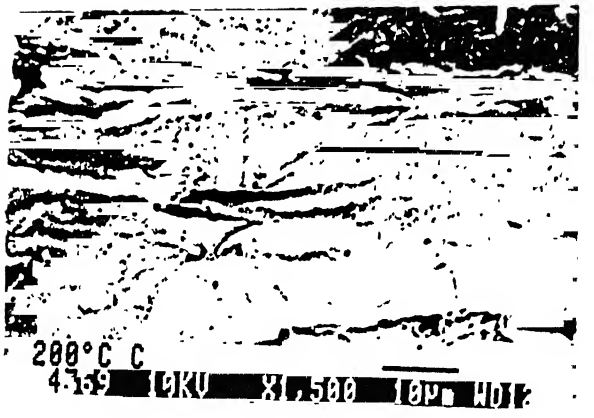

(a)

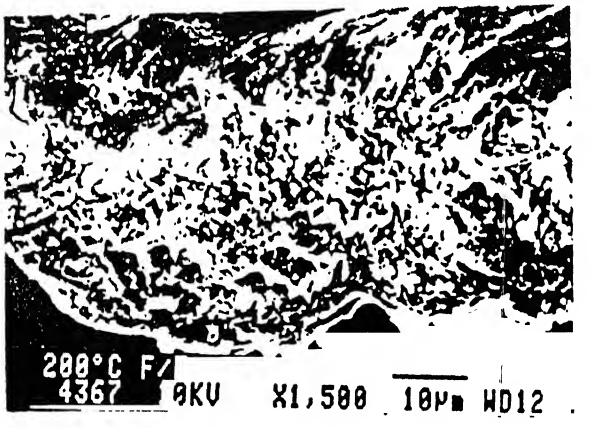

(b)

Figure 3.2 Micrographs of Al-SiC foam showing (a) surface characteristics (b) fractured edge. The sample had been previously been exposed to 200°C prior to microscopy

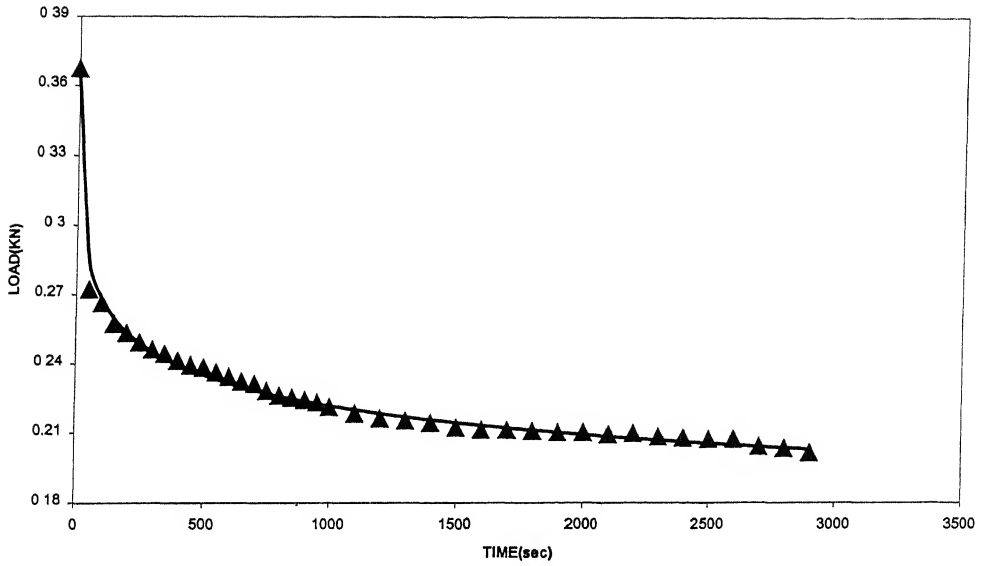

Figure 3.3 Creep relaxation curve of Al-SiC foam at T = 300°C and P_o = 0.367KN

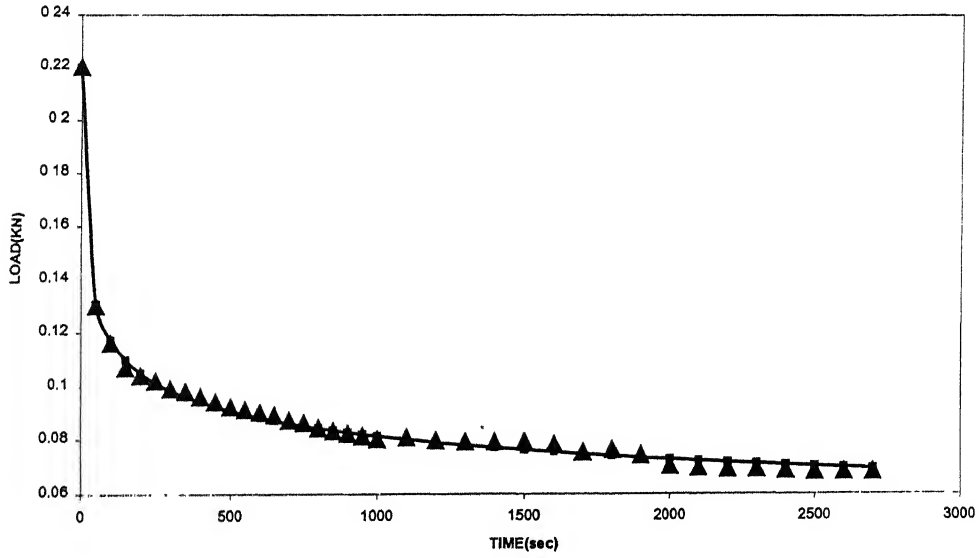

Figure 3.4 Creep relaxation curve of Al-SiC foam at T = 400°C and P_o = 0.22KN

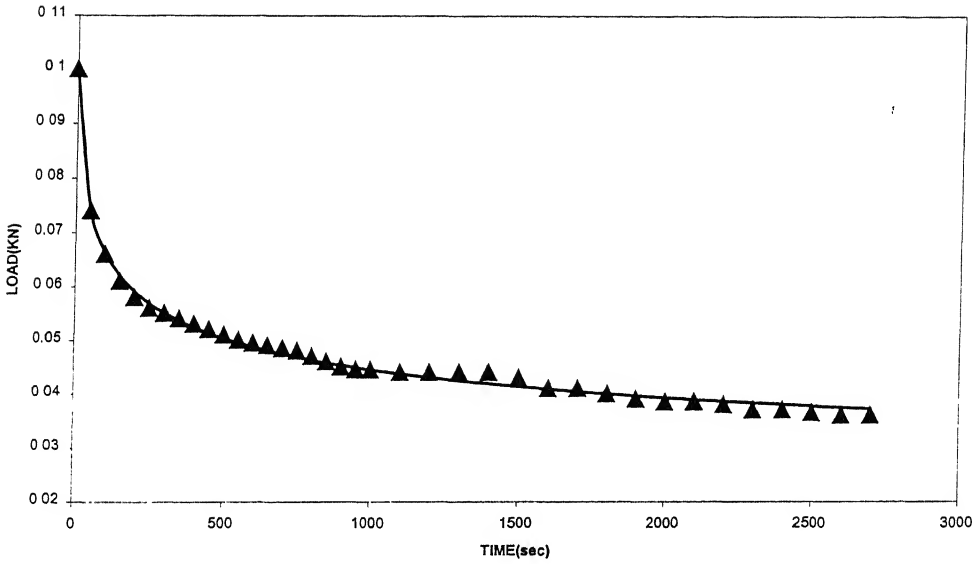

Figure 3.5 Creep relaxation curve of Al-SiC foam at T = 450°C and P_o = 0.1KN

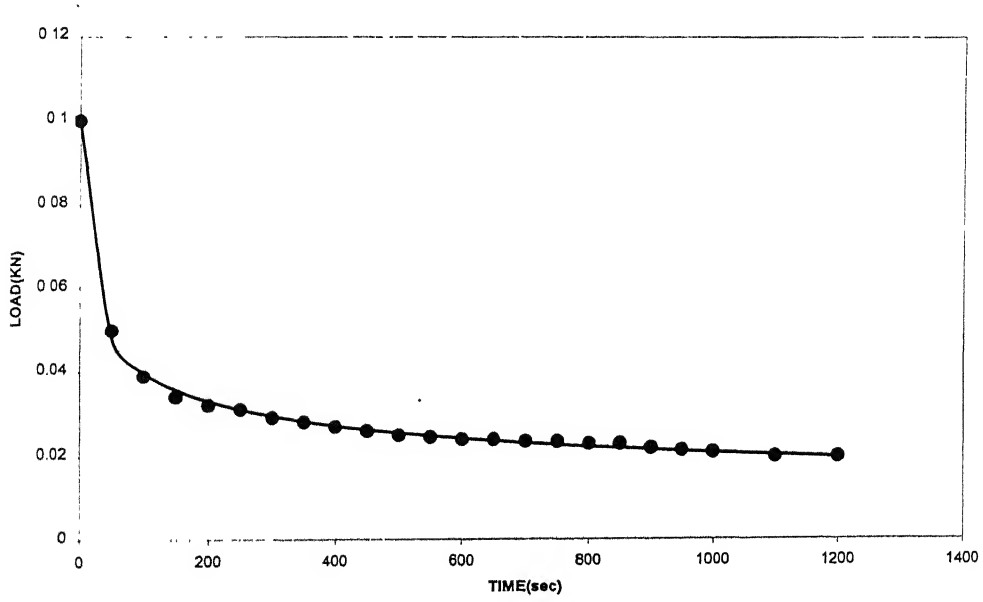

Figure 3.6 Creep relaxation curve of Al-SiC foam at T = 500°C and P_o = 0.1 KN

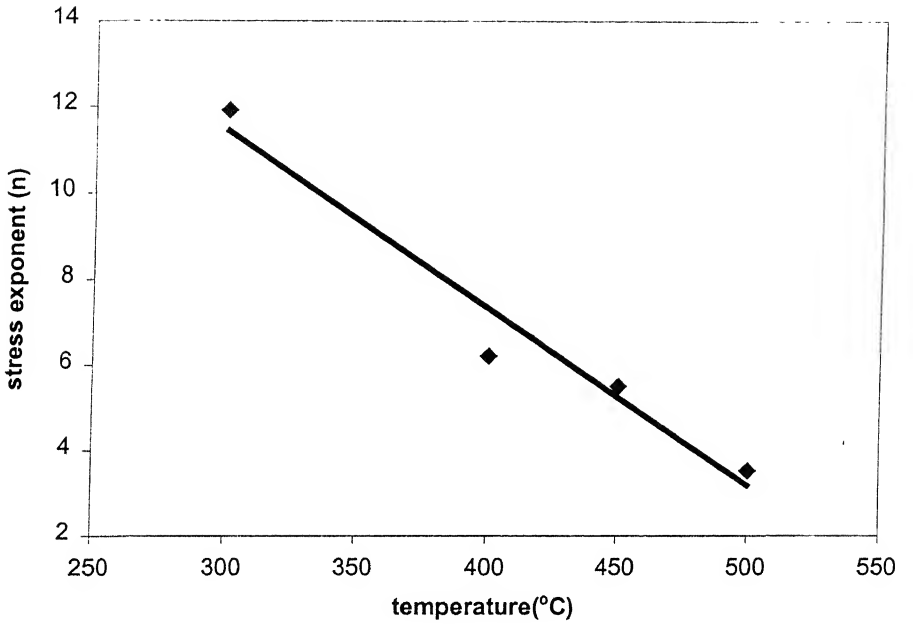

Figure 3.7 Variation of stress exponent with temperature

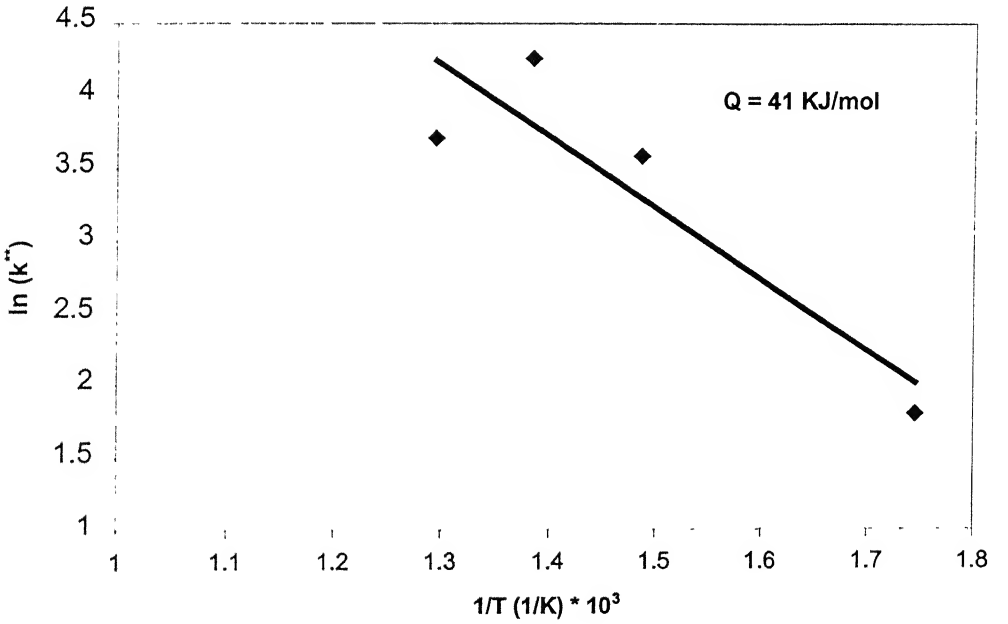

Figure 3.8 Arhenius plot showing ln (k**) vs. (1/T)

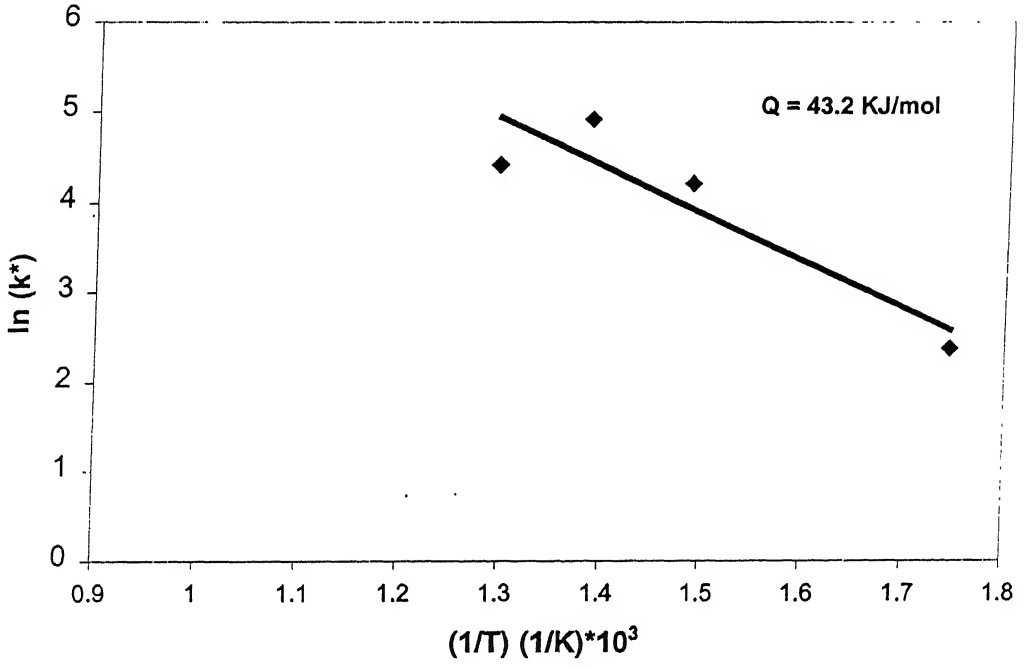

Figure 3.9 Arhenius plot showing ln (k*) vs. (1/T). Case: Temperature dependence of elastic modulus taken into consideration.

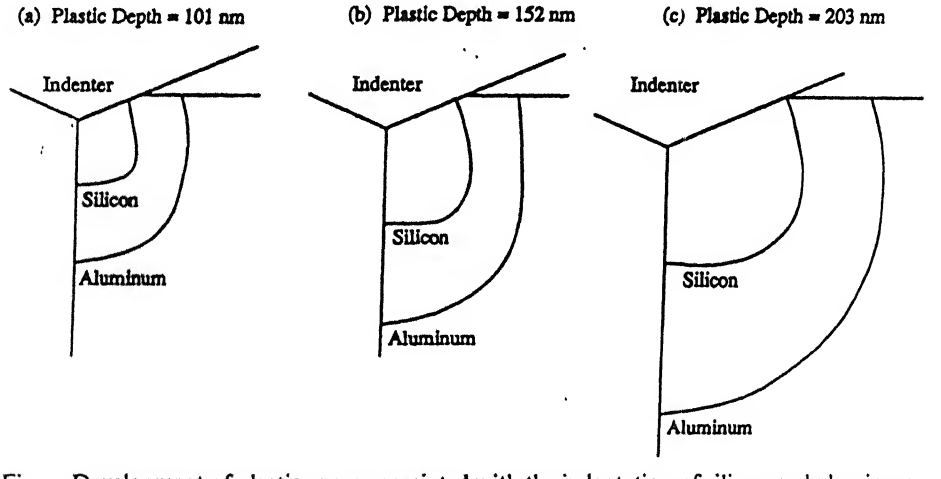

Fig Development of plastic zones associated with the indentation of silicon and aluminum.

CHAPTER 4

CONCLUSIONS

4.1 Conclusions

This work has centred about the indentation creep relaxation behaviour of Al-SiC foam. Al-SiC foam is a new class of cellular solid based on a metal matrix composite. Though some preliminary work has been reported on the mechanical properties of this material both at room temperature and elevated temperature, little is known about its response to contact stresses. Accordingly, this work has dealt with the high temperature mechanical response of Al-SiC foam under indentation loading.

Creep relaxation tests were conducted by indenting the material to a pre-specified load using a cylindrical punch indenter at various temperatures and the relaxation data obtained. Creep properties of cell wall material were extracted from the relaxation data using a theoretical formulation developed earlier for compression creep relaxation response of metallic foam. The use of this model for indentation creep relaxation has been discussed in relation to low Poisson's ratio and the expected shape of stress field in the material under punch indentation loading. Stress exponent values were obtained in the range 4-13, in close agreement with the properties of the cell wall material. These high values indicate the presence of threshold stress. The threshold stress appears due to load transfer to the particulates. The activation energy for creep is found to be 42 kJ/mole and indicates significant contribution of surface diffusion.

4.2 Future Work

The analysis of the indentation creep relaxation data was carried out using a model which had previously been developed for compression creep relaxation tests.

Although this issue has been discussed in relation to the low Poisson's ratio of cellular solids and the shape of the plastic zone under the indenter in a elastic-plastic half space, a more accurate estimate of the stress field should be carried out using FEM simulations. Also, it would be useful to test the validity of the theoretical approach used in this work against experimental studies on cellular solids based on other material – pure metals, polymers, and ceramics.

`References

[1] P. Schidrowitz and H.A. Goldsbrough, British Patent A, 111, 1914.

[2] M.C. Shaw and T.sata, *Int. J. Mech. Sc.*, 8, 1961, pp469.

[3] B.L. Ruskin, Hand Book of foamed Plastics, Lake Publishing, Libertyville, I11, 1965,Chap XIV.

[4] L.J. Gibsin and M.F. Ashby, Cellular Solids: Structures and Properties, Pergamon Press, Oxford, 1988.

[5] Shapovalov, Method for Manufacturing Porous articles, U.S. Patent No: 5 181 549, 1993.

[6] I. Jin, L.D. Kenny and H. Snag, U.S patent No: 5 112 697 1992.

[7] M.E. Rosa nad M.A.Fortes, *J. Mat. sc.*, 26, 1991, pp341.

[8] P.H. Thornton and C.L. Magee, Deformation of Aluminium Foams, Met. Trans., Vol. 6A, 1975, pp1253.

[9] L.J.Gibson, M.F Ashby, J. Zhang and Triantafillou, *Int. J. Mech. Sc.*, 31,1989, pp635.

[10] M.F. Vaz and M.A. Fortes, *J. Mat. Sc. Lett.*, 12, 1993, pp1408.

[11] O. Prakash, H. Snag and J.D. Embury, Structure and Properties of Al-Sic Foam, *Mat. Sc. & Engg.*, A 199, 1995, pp195.

[12] G. A. Ansell and Weertman, *Trans.* AIME, 215, 1959, pp838.

[13] R. Lagneborg, *J. Mater. Sci.*, 3, 1968, pp596.

[14] S.K Mitra and D. Melean, *Proc. Roy. Soc.*, A295, 1966, pp288.

[15] R.S.W. Shewfelt and L.M. Brown, *Phil. Mag.*,30,1974,pp1135

[16] J.H. Hausselt and W.D. Nix, *Acta Met.*, 25, 1977, pp596.

[17] E. Arzt and D.S. Wilkinson, *Acta Met.*, 34, 1986, pp1893

[18] T.G. Nieh, Creep Rupture of a SiC Reinforced Aluminium Composite, *Met. Trans.*, Vol. 15A, 1984, pp139.

[19] H. J. Frost and M.F. Ahsby, Deformation Mechanism Maps, Pergomon Press, 1982.

[20] C.L. Myres, J.C. Shyne and O.D. Sherby, Relation of Properties to Structure in Sintered Aluminium Powder, *J. Austral. Inst. Metals*, 8, 1963, pp171.

[21] A.B. Pandey, R.S. Mishra and Y.R. Mahajan, *Acta Metall. Mter.*, Vol. 40, 1992, pp2045.

[22] O. Prakash, Unpublished Results.

[23] I. Finnie and W.R. Heller, Creep of Engineering Materials, McGraw Hill, !959.

[24] A. C. F Cocks and A.R.S. Ponter, Mechanics of Creep Materials – 1, Elseivier Applied Science Publishers Ltd., 1989.

[25] B. Harris, Engineering Composite Materials, The Institute of Metals, 1986, London.

[26] T. Morinto, T. Yamaoka, H. Lilholt and M. Taya, *J. Engg. Mater.* Technol., Vol. 110, 1988, pp70.

[27] A.B. Pandey, R.S Mishra and Y.R. Mahajan, *Meta. & Mat. Trans.*, Vol.27A, 1996, pp305.

[28] O. Prakash, PhD. Thesis, Cambridge Univ., 1992.

[29] Prathyush khare, M.Tech. Thesis, I. I.T. Kanpur. 1998.

[30] Bhattacharaya and Nix, Int. J. Solids Structures Vol. 27, No. 8, 1991, pp. 1047-1058.

[31] Freund L.B, Int. J. Solids structures, 32, 1995, pp 911-923.

Appendix A

Creep Relaxation in uniaxial loading of Cellular Solids

A model for Creep Relaxation of cellular solids under compression loading was developed in [29] and the salient points are outlined here. The model relates the creep relaxation behavior of a cellular solid in terms of the creep properties of the cell-wall material. Some simplifying assumptions are made regarding the role of various structural members in such materials. As discussed in [11], cell walls bear most of the load (in comparison to the cell membranes) the structure can be assumed to consist of a skeleton of beam elements. The overall response of the material can then be obtained by integrating (summing) the response of individual beam elements. Because of the cell-geometry and the manner in which load is transferred from one cell to another (see figure A1), a cell wall can be idealized to be a cantilever beam experiencing a point load at the tip.

Elastic bending of the beam is then considered in conjunction with their creep deformations. The cell walls material is assumed to follow a power-law type creep behavior. Shear deflections are neglected by assuming the beams to be long compared to their cross-section. Similarly strain component resulting from axial compression of beam element is negligibly small compared to strain component due to bending.

Now, in creep relaxation, part of the elastic strain is converted to creep strain resulting in relaxation of elastic stresses. The total strain (elastic + creep), however, remains constant. Therefore,

$$\delta_e + \delta_c = \text{constant} \qquad \text{A.1}$$

Where, δ_e is the elastic deflection due to creep processes. Considering displacement rates, i.e. taking the rate form of the above equation,

$$\dot{\delta}_e + \dot{\delta}_c = 0 \qquad \text{A.2}$$

Where, the notation $\dot{\delta}$ denotes time derivative

Creep in cellular materials is associated with creep bending of cell-walls. For a tip loaded cantilever (figure A2) the elastic deflection is given by:

$$\delta_e = \frac{PL^3}{3EI} \qquad \text{A.3}$$

where,

P = load

L = length of beam element

E = elastic modulus

I = moment of inertia of the beam section for a regular cross-section, which is $bt^3/12$

where,

b = width of the beam

t = thickness of the rectangular section.

Again, considering deflection rate. We obtain:

$$\dot{\delta}_e = \frac{\dot{P}L^3}{3EI} \qquad \text{A.4}$$

Deflection rate $(\dot{\delta})$, is the creep rate of tip loaded cantilever made of a material obeying power law creep is given by [23]:

$$\dot{\delta}_c = \frac{2\varepsilon_0 L}{(n+2)}\left[\frac{(2n+1)}{n} \times \frac{P}{bt}\right]^n \left(\frac{L}{t}\right)^{(n+1)} \qquad \text{A.5}$$

Where,

n = power-law creep stress exponent of the beam material

P= applied load

L= length of the beam

ε_0 = creep constant for a material at a given temperature

The power law creep equation is:

$$\dot{\varepsilon} = \varepsilon_0 \sigma^n = a\sigma^n \exp\left(\frac{-Q}{RT}\right) \qquad \text{A.6}$$

Where,

a = a constant

σ = Stress

Q = activation energy for creep

R = Universal gas constant

T = Temperature,

As discussed in chapter one, creep of solid metal-matrix-composites is described well (phenomenological) by a power law equation.

In order to account for simultaneous deformation of many beam elements (cell walls) with a distribution in length (l_i), orientation (θ_i), cross-sectional area (A_i) and the dimensions b_i anf h_i in a foam sample, we invoke equilibrium and compatibility conditions. Depending on the variation in these parameters, individual beam elements at a given cross-section will bear some part (P_i) of the load (P). This can be represented as:

$$P = \sum P_i \qquad \text{A.7}$$

For strain compatibility, we get:

$$\delta_c = \delta_i \qquad \text{A.8}$$

Differentiating for the rate form of the above equation:

$$\dot{\delta}_c = \dot{\delta}_i \qquad \text{A.9}$$

let L_i denote $l_i cos\theta_I$. From equations (3.5) and (3.7):

$$P = \sum P_i = \sum \dot{\delta}_c^{\,1/n} . T_i = \frac{\dot{\delta}_c^{\,(1/n)}}{\varepsilon_0^{\,(1/n)}} \sum T_i \qquad \text{A.10}$$

where,

$$T_i = \frac{n}{2n+1}\left(\frac{t_i}{l_i}\right)\left(\frac{n+1}{n}\right).\frac{t_i}{l_i}.\frac{1}{n+1}.\frac{b_i t_i}{(L_i)(1/n)}.\left(\frac{n+2}{2}\right)\left(\frac{1}{n}\right).(\cos\theta_i)\left(\frac{n+2}{n}\right) \qquad \text{A.11}$$

the above equation consists of term n, which describe material property and beam (cell-wall) statistics t_i, l_i, b_i, θ_I. Rearranging equation (A.11),we get:

$$\dot{\delta} = \frac{P^n}{(\Sigma T_i)^n} \varepsilon_0 \qquad \text{A.12}$$

Substituting the values of $\dot{\delta}_e$ *and* $\dot{\delta}_c$ from equation A.12 into equation (a.2) we get:

$$\frac{dP}{dt} G = \frac{P^n}{(\Sigma T_i)^n} \varepsilon_0 \qquad \text{A.13}$$

where,

$$G = \left(\frac{l^3 \cos^3 \theta}{3EI}\right) \qquad \text{A.14}$$

Since the terms G and ΣT_i depend upon material properties (n, ε_0, E) and statistics on cell geometry (t_i, l_i, b_i), they are likely to be constant for all samples from a given batch of foam. This assertion is supported by the simulation of work described in section A.3 thus, integrating equation A.13, we get:

$$\frac{1}{P^{n-1}} - \frac{1}{P_0^{n-1}} = kt \qquad \text{A.15}$$

Where,

$$\frac{1}{k} = \frac{l_i^3 \cos^3 \theta_i}{3EI} \exp\left(\frac{Q}{RT}\right) \cdot \frac{1}{n-1} \cdot \frac{1}{a} \cdot \Sigma \left(\frac{n}{2n+1}\right)^n \left(\frac{n+2}{2}\right)^n \cdot \frac{n+2}{2} \cdot \left(\frac{t_i}{l_i}\right)^{n+1} \cdot (b_i t_i)^n \cdot \frac{1}{l_i} \cdot \qquad \text{A.16}$$

where,

Q = Activation energy of creep for cellular solid

R = Universal gas constant (8.314J/mole K)

T = temperature in K

Denoting n – 1 = m, in equation (A.15), we finally get:

$$\frac{1}{P^m} - \frac{1}{P_0^m} = kt \qquad \text{A.17}$$

where,

k = a material constant

P_0 = initially applied load at t=0

P = instantaneous load at time, t

m = stress exponent of cellular solid

The stress exponent 'm' can be derived by fitting experimental data to equation A.17. The stress exponent should correspond to the power-law creep stress exponent for uniaxial creep of solid cell wall material (i.e. n= m+1).

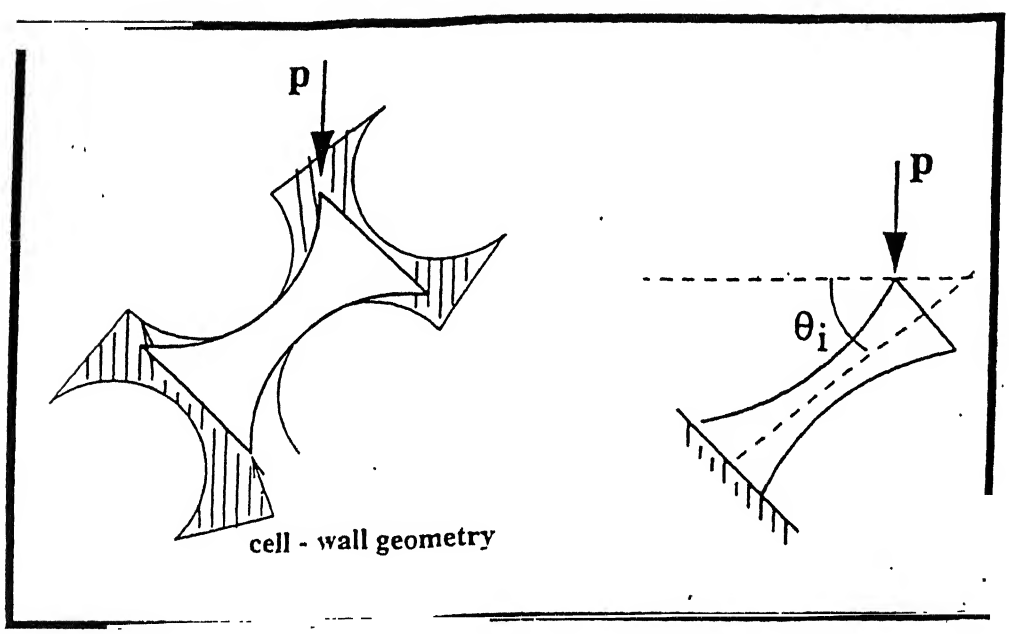

Figure A.1 Idealization of cell geometry as a tip loaded cantilever.

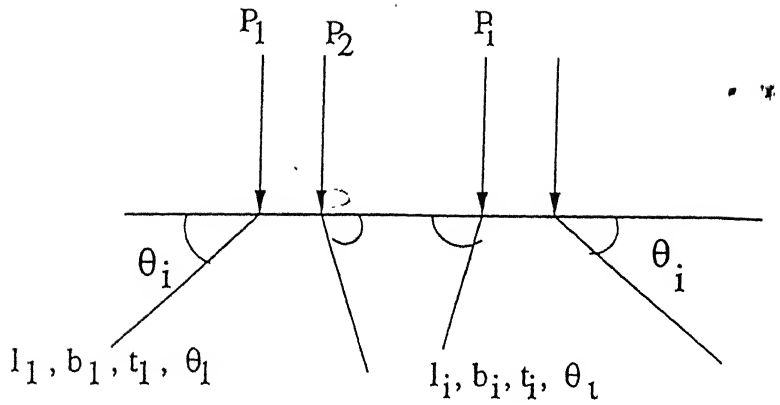

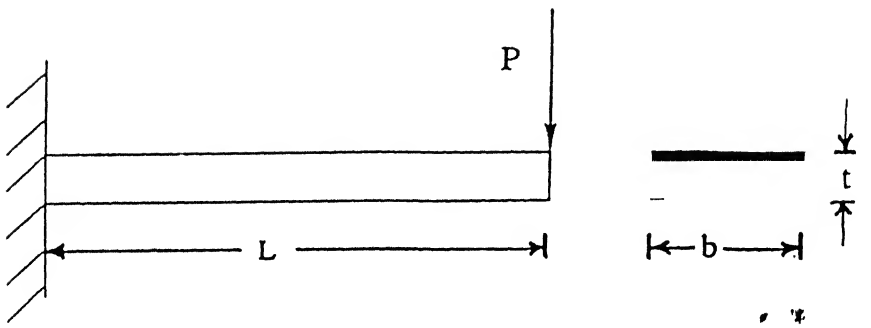

Figure A.2 (A) Schematic diagram of the idealized loading geometry: cantilever with a point load at one end. (B) Nomenclature of cell-wall statistics.

Appendix B

Determination of Activation Energy

From equation A.16, we have:

$$\frac{1}{k}=\frac{l_i^3\cos^3\theta_i}{3EI}\exp\left(\frac{Q}{RT}\right)\frac{1}{n-1}.\frac{1}{a}.\Sigma\left(\frac{n}{2n+1}\right)^n.\left(\frac{n+2}{2}\right).\left(\frac{t_i}{l_i}\right)^{n+1}(b_i t_i).\frac{1}{l_i} \qquad \text{B.1}$$

The above equation can also be written as,

$$\mathrm{k} = J f(n)\, E \exp\left(\frac{-Q}{RT}\right) \qquad \text{B.2}$$

where,

J = geometrical term

$$f(n)=\left(\frac{2n+1}{n}\right)^n.\frac{n-1}{n-2} \qquad \text{B.3}$$

If n remains constant over a given (small) temperature interval is independent of temperature and can also be considered constant.

Now, elastic modulus (E) is also a function of temperature (although a weak function) [19] and if f (n) is also temperature dependent, then activation energy can be found as follows:

$$\mathrm{k}^* = \frac{k}{f(n)E}=J\exp\left(\frac{-Q}{RT}\right) \qquad \text{B.4}$$

Thus,

$$\ln(k^*)=\ln(J)-\left(\frac{Q}{RT}\right) \qquad \text{B.5}$$

Therefore, activation energy is given by the slope of a plot between ln(k*) vs. 1/T.If the temperature dependence of E is taken to be negligibly small, we obtain, in a similar fashion,

$$\ln(k^{**})=\ln(JE)-\frac{Q}{RT} \qquad \text{B.6}$$

where, $k^{**}=k/f(n)$

Appendix C

Relation between linear, surface and volume density of cellular solids:

Consider volume comprising of N^3 cells (N cells to a side). If n cells along each side are filled, the linear density will be

$$f_L = \frac{n}{N} \qquad \text{C.1}$$

The surface and volume densities will be given by

$$f_{Surface} = \left(\frac{n}{N}\right)^2 \qquad \text{C.2}$$

$$f_{vol} = \left(\frac{n}{N}\right)^3 \qquad \text{C.3}$$

Hence, $f_{surface} = (f_{vol})^{2/3}$ C.4

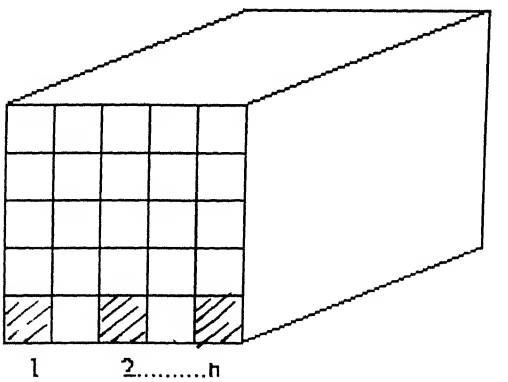

133672

Date Slip

The book is to be returned on the date last stamped.

.....	.....
.....	.....
.....	.....
.....	.....
.....	.....
.....	.....
.....	.....
.....	.....
.....	.....
.....	.....
.....	.....
.....	.....